A Model Based DC Fault Location Scheme for Multi-terminal MMC-HVDC Systems Using a Simplified Transmission Line Representation

Jianzhong Xu, *Member, IEEE*, Yu Lü, Chengyong Zhao, *Senior Member, IEEE* and Jun Liang, *Senior Member, IEEE*

Abstract—**Accurately determining the location of DC pole-to-pole short-circuit faults in modular multilevel converter (MMC) based multi-terminal HVDC (MTDC) systems is key issue in ensuring fast power recovery. This paper proposes an effective DC fault location scheme for the MMC-MTDC that uses an estimated R-L representation of the transmission lines. By using the measured voltage and current data from both ends of the faulted DC line, the proposed fault location formulas can calculate the location of the fault with high accuracy. The simplified R-L representation greatly reduces the computation burden of the fault detection algorithm. Electromagnetic transient (EMT) simulations of a four-terminal MMC-MTDC system on PSCAD/EMTDC are used to confirm the effectiveness of the proposed approach. The results verify that the proposed scheme is robust and almost not affected by the transmitted power or the fault resistance.**

Index Terms—**Modular multilevel converters (MMC), fault location scheme, multi-terminal HVDC system; simplified transmission line representation.**

I. INTRODUCTION

HIGH Voltage Direct Current (HVDC) transmission system employing modular multilevel converter (MMC) is an effective solution to transfer the fluctuating renewable source energies through long distance overhead lines [1]-[3]. Due to its advanced features such as almost harmonic free waveforms and better scalability, MMC has been applied in building large scale multi-terminal HVDC (MTDC) grid [4]. The DC fault protection schemes such as fault detection, isolation, location, fault clearance, and fast recovery can ensure continuous operation and desired performance of the MTDC grid. Among these aspects, the DC fault location scheme is beneficial to accelerate the fault clearance and power recovery processes and will reduce the duration of power interruption [5].

In recent years, a large number of methods to detect and locate DC faults have been proposed, which can be classified into two categories, respectively, the travelling-wave methods [6]-[10] and time-domain location methods [11]-[14]. The basic principle of traveling-wave method is to determine the measurement point and calculate the propagation distance based on the arrival time of the wave front and the propagation velocity [15]. The time-domain location method calculates the voltage and current distributions along the transmission line by using voltage and current measured at both ends [16]. Then the fault location can be obtained by using the wave equation and the electrical characteristics of the fault point.

The travelling-wave based methods can be applied to both AC and DC lines to locate faults and are usually considered as powerful techniques for the latter [17]. Extensive studies have proven that it is feasible to locate fault merely by using the arrival time of travelling waves at different locations. Reference [6] only needs the initial time that the traveling waves reach all terminals to determine the fault occurring time (FOT) of the shortest paths between any two terminals, and the smallest one indicates the fault location. Thanks to the global positioning system (GPS), all the MMC terminals can share a common clock signal with a time synchronization accuracy of less than 0.1μs [7]. In those methods, high sampling frequency is needed to identify the wave head accurately which is a key issue to locate the fault. However, it is hard to detect the fault if the fault resistance is large or the fault is caused by a gradually changing fault resistance, due to the fact that the travelling waves become too weak under these circumstances [28].

In order to exclude the influences of the fault and disturbance characteristics of power system, the Wavelet Transform (WT), as an effective method for analyzing sudden changes in input signals, has been widely applied [8]-[9], with the aim of improving the accuracy of detecting the arrival of travelling waves. Reference [10] proposed a two-terminal fault location approach which analyses aerial mode travelling waves and incident ground without using propagation velocity of travelling wave and the data synchronization. However, the application of the algorithm is limited to ground faults only. The WT-based methods can be of high accuracy, with most of the relative error within 1% [6], [7], [10]. As stated above, the accuracy of these location schemes largely depends on the accurate detection of the surge arrival time and the wave speed [16]. However, the wave head is hard to capture and the

propagation velocity can be affected by transmission line parameters [18].

The time-domain fault location methods, which use the distributed parameter model of the DC transmission lines, can obtain correct fault point from collected data [11], [12]. Due to the use of voltage and current signals, the location accuracy is affected by the differences in the transfer characteristics of the voltage transformer (VT) and the current transformer (CT), and thus the secondary voltage and current cannot strictly satisfy the differential equation, which will reduce the accuracy of the fault location [15]. Reference [13] applies the WT method and principal component analysis to extract the characteristics information from local DC current measurement as input to the genetic fuzzy system. It can reduce the impact of the transmission error of the transformer to some extent. Reference [14] applies the Pearson correlation coefficient to measure the similarity between the newly sampled voltage signals and the existing ones for DC fault location. Although these algorithms do not improve the model accuracy substantially, the ranging result can be corrected. Therefore, more accurate time-domain location schemes are required. The simplified representation of the transmission lines is important input for accurate theoretical analysis of HVDC system, e.g. [24] and [27] used such lumped parameters for DC-side short-circuit fault current calculation of MMC-HVDC grid. Although the results seen to be accurate within several milliseconds after the fault, the method to obtain these equivalent parameters of the transmission line are not provided, thus limits their application for other purposes such as the fault location in this paper.

To address this issue, this paper proposes a DC fault location method for MMC based MTDC systems, which is based on the estimated R-L model of the frequency dependent transmission line (FDTL). Compared with traveling wave methods requiring a high sampling frequency [29], [30], the proposed algorithm can achieve similar accuracy with a lower sampling frequency. When comparing with the exiting time domain methods, the new approach only needs the voltage and current information from two terminals of the faulted line and no need for the additional algorithms of large complexity to improve the location accuracy, hence the algorithm is simple and reliable.

II. Four-terminal MMC-HVDC System and The Fault Location Scheme

A. The Topology of MMC and MTDC System

The classical half-bridge MMC shown in Fig. 1 is used as basic converter topology. The four-terminal and true bipolar MMC-MTDC system shown in Fig. 2 is used as the benchmark model [19], with the transmission lines based on the FDTL model [20].

Fig. 1 The half-bridge MMC.

Fig. 2 The four-terminal MMC-MTDC system.

B. Fault Location Scheme

In Fig. 2, DC short-circuit faults can occur at any location of the arbitrary DC lines, and the faults can be either single-pole or pole-to-pole faults. The proposed fault location scheme in this paper is suitable for both types of DC faults, and the pole-to-pole fault will be used to exemplify the basic location algorithms. The entire flow chart of the algorithm is shown in Fig. 3, which includes three blocks.

Fig. 3 The flowchart of the proposed DC fault location scheme.

The DC short-circuit faults are continuously detected, and the DC voltage and current data from both ends of any line are continuously stored in a sliding window manner. Then the following three blocks will implement the location algorithm.
● Block 1: Detection of Fault Initiation Algorithm.

$$\nabla U_j(k) = \sum_{i=1}^{3} U_{mn\_j}(k-i) - \sum_{i=4}^{6} U_{mn\_j}(k-i) \quad (1)$$

$$\left|\nabla U_p(k)\right| > U_{set} \quad \& \quad \left|\nabla U_n(k)\right| > U_{set} \quad (2)$$

The voltage data U_{mn_j} will be fed into the voltage gradient algorithm [21] and if the voltage gradients ∇U_p and ∇U_n exceed the preset value U_{set}, it is determined that pole-to-p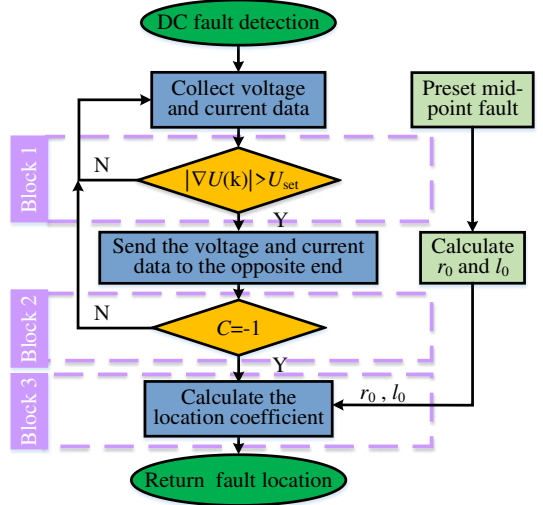ole fault has occurred. Note that k represents the sampling point, k-i is the i_{th} sampling point prior to the present moment, $j=p,n$.

● Block 2: Fault Type Classification.

$$\begin{cases} \Delta I_{mn} = I_{mn} - I_{mn0} \\ \Delta I_{nm} = I_{nm} - I_{nm0} \end{cases} \quad (3)$$

$$C_{ia}\left(\Delta I_{mn}, \Delta I_{nm}\right) = \frac{\sum_{k=1}^{n} \Delta I_{mn}(k) \cdot \Delta I_{nm}(k)}{\sqrt{\sum_{k=1}^{n} \Delta I_{mn}^{2}(k)} \sqrt{\sum_{k=1}^{n} \Delta I_{nm}^{2}(k)}} \quad (4)$$

Current-deviations ΔI_{mn} and ΔI_{nm} can be calculated by using fault current I_{mn}, I_{nm} and pre-fault currents I_{mn0}, I_{nm0}. Feeding ΔI_{mn} and ΔI_{nm} into the included angle cosine C_{ia}, if C_{ia} is close to "-1", internal fault is distinguished. n represents the number of sampling points. In this paper as the sampling frequency is 50 kHz and the data window is 5ms, the size of 'n' is 250.

● Block 3: Identification of Fault Location. The voltage and current data are fed into the proposed location coefficient to calculate the fault location. During the calculation, the estimated R-L model parameters of transmission line will be used, which are obtained from preset fault test.

The main contribution of this paper relies on Block 3, which will be described in detail in Section III and Section IV.

III. IDENTIFICATION OF FAULT LOCATION

There are three stages in the development of pole-to-pole faults, with the capacitors fast discharging being the first [23]. At this stage, the individual MMC can be equivalent to a second-order RLC circuit. However, obtaining the analytical solution of the voltage and current data in the MMC-MTDC system is extremely difficult due to the strong coupling of the discharging processes of all the terminals [24].

To address this issue, the measurement values of the voltages and currents from each terminal are used for fault location, which are captured from the FDTL model-based DC network and has considered the detailed characteristics of the actual transmission lines. The equivalent circuit of the estimated R-L model-based DC fault discharging process is shown in Fig. 4. The actual voltage and current data are filtered by a first-order lag to eliminate the influence of high frequency components caused by distributed capacitance parameters. Hence the distributed capacitance is not included in the calculation.
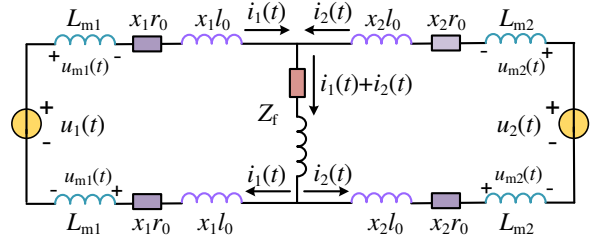

Fig. 4 The estimated R-L equivalent circuit in first stage of pole-to-pole short-circuit fault.

In Fig. 4, $u_1(t)$ and $u_2(t)$ represent the actual measurement values of DC voltages at the DC bus bars of the converters; the variables $i_1(t)$ and $i_2(t)$ represent the discharging currents of the MMC capacitors from both terminals; The variables $u_{m1}(t)$ and $u_{m2}(t)$ indicate the actual measurement values of the voltage drop on smoothing reactors at both ends of the line; L_{m1} and L_{m2} are respectively smoothing reactors close to terminal "1" and "2"; Z_f represents the fault resistance; x_1 and x_2 respectively indicate the distances from the fault point to the left and right ends of the inverter bus bar; The variable r_0 is the resistance per unit length of the line and l_0 is the inductance per unit length. Note that r_0 and l_0 are the equivalents derived from the FDTL model which are used for fault location analysis and will be provided in later subsection.

In Fig. 4, the internal structures of the two terminal converters are not considered, instead the terminal voltage and current are measured in real time, hence the equivalent circuit in Fig. 4 and the following equations are both applicable to other VSC configurations. Based on the equivalent circuit in Fig. 4, apply KVL and KCL to both circuits, equations (5) and (6) can be obtained:

$$2L_{m1}\frac{di_1(t)}{dt} + 2r_0 x_1 i_1(t) + 2l_0 x_1 \frac{di_1(t)}{dt} + \left[i_1(t) + i_2(t)\right]Z_f = u_1(t) \quad (5)$$

$$2L_{m2}\frac{di_2(t)}{dt} + 2r_0 x_2 i_2(t) + 2l_0 x_2 \frac{di_2(t)}{dt} + \left[i_1(t) + i_2(t)\right]Z_f = u_2(t) \quad (6)$$

Subtracting of the above two equations can eliminate the effect of fault resistance, and thus (7) is obtained:

$$\begin{aligned} & u_1(t) - u_2(t) - 2L_{m1}\frac{di_1(t)}{dt} + 2L_{m2}\frac{di_2(t)}{dt} \\ & = x_1\left[2r_0 i_1(t) + 2l_0 \frac{di_1(t)}{dt}\right] - x_2\left[2r_0 i_2(t) + 2l_0 \frac{di_2(t)}{dt}\right] \end{aligned} \quad (7)$$

Let L be the total length of the faulted line, then

$$x_1 + x_2 = L \quad (8)$$

Define $\lambda = \dfrac{x_1}{L}$ to be the ratio of the distance from the fault point to the corresponding terminal over the total length of the DC line, then substituting (8) to (7) yields

$$\lambda = \frac{L\left[2r_0 i_2(t) + 2l_0 \dfrac{di_2(t)}{dt}\right]}{L\left[2r_0 i_1(t) + 2l_0 \dfrac{di_1(t)}{dt} + 2r_0 i_2(t) + 2l_0 \dfrac{di_2(t)}{dt}\right]}$$
$$+ \frac{u_1(t) - u_2(t) - 2L_{m1}\dfrac{di_1(t)}{dt} + 2L_{m2}\dfrac{di_2(t)}{dt}}{L\left[2r_0 i_1(t) + 2l_0 \dfrac{di_1(t)}{dt} + 2r_0 i_2(t) + 2l_0 \dfrac{di_2(t)}{dt}\right]} \quad (9)$$

In order to decrease the rate of rising of the DC fault current, the MTDC systems are usually equipped with smoothing reactors, then voltage drop across the reactor can be expressed as

$$u_{m1,2}(t) = L_{m1,2} \frac{di_{1,2}(t)}{dt} \quad (10)$$

Thus, the current derivative can be calculated by the voltage change of the smoothing reactor without substitution errors caused by differential calculations [25], i.e.

$$\frac{di_{1,2}(t)}{dt} = \frac{u_{m1,2}(t)}{L_{m1,2}} \quad (11)$$

Substituting (11) to (9), the time domain expression of λ can be obtained as (12), which depends on the actual measurement values and the estimated DC line parameters to locate faults.

$$\lambda(t) = \frac{L\left[2r_0 i_2(t) + 2l_0 \dfrac{u_{m2}(t)}{L_{m2}}\right]}{L\left[2r_0 i_1(t) + 2l_0 \dfrac{u_{m1}(t)}{L_{m1}} + 2r_0 i_2(t) + 2l_0 \dfrac{u_{m2}(t)}{L_{m2}}\right]}$$
$$+ \frac{u_1(t) - u_2(t) - 2u_{m1}(t) + 2u_{m2}(t)}{L\left[2r_0 i_1(t) + 2l_0 \dfrac{u_{m1}(t)}{L_{m1}} + 2r_0 i_2(t) + 2l_0 \dfrac{u_{m2}(t)}{L_{m2}}\right]} \quad (12)$$

Three short-circuit fault locations are applied on Line 1 of the FDTL model based MMC-MTDC system shown in Fig. 2, the fault occurs at time $t = 1s$, and the fault distances from the converter station S_1 are respectively 10%, 50%, and 90% of the total line length. The corresponding voltage and current simulation results for each fault point are independently used to calculate λ after passing through the first-order filter, with the results shown in Fig. 5.
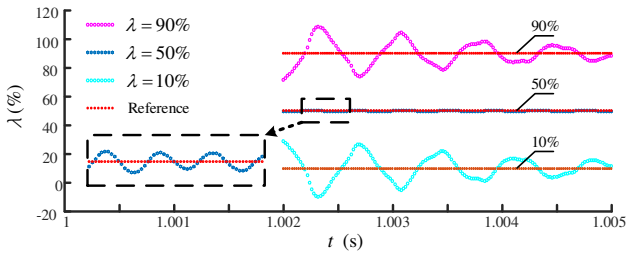

Fig. 5 The calculated λ for different fault locations.

The first-order filter can eliminate the interference caused by high-frequency components, it cannot completely remove the ripples of the voltages and currents, which will make the calculated λ fluctuate along the time axis. Fortunately, as shown in Fig. 5, the calculated λ fluctuates around the reference value within 2ms to 5ms after the fault. In order to account for this issue, a fault location coefficient η is defined to obtain the averaged value of fluctuations, which is the value with the minimum square sum of distances to the calculated λ corresponding to all the sampling times. According to the physical meaning, η is within the range of 0 to 1 and satisfies (13).

$$\min \sum_{k=1}^{n} \left[\lambda(k) - \eta\right]^2 \quad (13)$$

The location algorithm uses the calculated η to quantitatively determine the fault location.

IV. THE ESTIMATED R-L MODEL

Formulas (12)-(13) need both the measured voltage, current data and the equivalent line parameters r_0 and l_0 which form the estimated R-L model. r_0 and l_0 can be determined through a fault test.

Referring to Fig. 4, the preset fault is set to be a pole-to-pole short-circuit fault occurring at the midpoint of the line without fault resistance. (14) gives the estimation method of the DC line parameters r_0, l_0, which applies KVL to the loop circuit formed by one terminal of the line and the fault point.

$$u_1(t) - 2u_{m1}(t) = 2r_0 L_{test} i_1(t) + 2l_0 L_{test}\frac{di_1(t)}{dt} \quad (14)$$

L_{test} represents the distance between the preset fault location and the terminal of the line. The r_0 and l_0 parameters of the line can be readily calculated by (14) written in different time intervals [26], and the matrix form containing r_0 and l_0 is given in (15).

$$\begin{bmatrix} u_1(t) - 2u_{m1}(t) \\ u_1(t+\Delta t) - 2u_{m1}(t+\Delta t) \end{bmatrix} = \begin{bmatrix} 2L_{test} i_1(t) & \dfrac{2L_{test} u_{m1}(t)}{L_{m1}} \\ 2L_{test} i_1(t+\Delta t) & \dfrac{2L_{test} u_{m1}(t+\Delta t)}{L_{m1}} \end{bmatrix} \begin{bmatrix} r_0 \\ l_0 \end{bmatrix} \quad (15)$$

In (15), Δt represents the time interval and all the voltage and current data have passed through the first-order lag first. Both r_0 and l_0, which are in the time domain, are calculated off-line. By setting pole-to-pole faults at the midpoint of the Line, the calculated r_0 and l_0 using (15) are shown in Fig. 6.
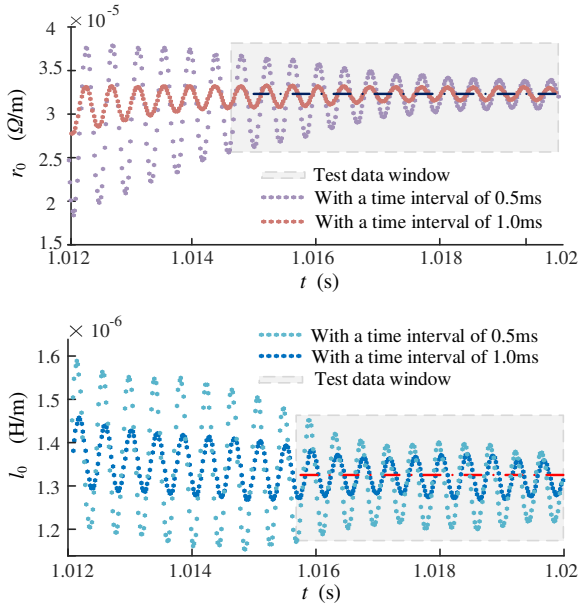
Fig. 6 Calculated r_0 and l_0 for the transmission line with different time intervals.

Similar to Fig. 5, the waveforms in Fig. 6 fluctuate around a certain value, and data fluctuation becomes small after 15ms. Then the data from 15ms to 20ms are used to obtain more stable and accurate r_0 and l_0. In order to wait for sufficiently long time until the data fluctuation decreases so that accurate r_0 and l_0 of the RL model can be obtained, the DCCBs are disabled in the process of identifying the RL model.

Time intervals value is a key parameter to equation (15) and for the fault location method. By comparison, the time interval is selected as 1.5ms, a relatively minimum location error can be obtained. After calculation, the results of r_0 and l_0 are respectively $3.3597 \times 10^{-5}\,\Omega/\text{m}$ and $1.2751 \times 10^{-6}\,\text{H/m}$.

To verify the model accuracy, values of r_0, l_0 are varied and associating location errors are calculated. Here the calculated line parameters in Section IV are used as reference values, i.e. $r_0=3.3597 \times 10\text{-}5\,\Omega/\text{m}$ and $l_0=1.2751 \times 10\text{-}6\,\text{H/m}$. Fig. 7 and Fig. 8 show the test results corresponding to different fault locations (f_1-f_4) of Line 1.
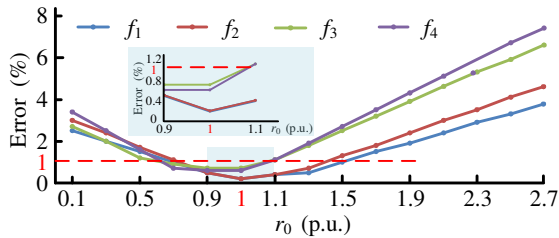

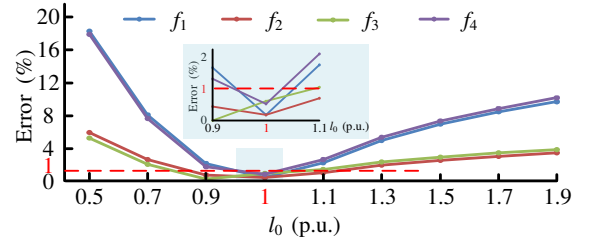Fig. 7 Location error varies with r_0

Fig. 8 Location error varies with l_0

The test results show that only when the r_0 and l_0 take values near the calculated value, they have the lowest location error which can be controlled within 1%. Perform the same test on Line 4 can get the similar results. It is enough to show that the R-L model has high accuracy, and r_0, l_0 can accurately reflect the short-circuit fault characteristics of the transmission line.

The DC system has no fundamental frequency, so it is difficult to use the phasor form to calculate the equivalent impedance of the fault. Also, the AC transmission line parameter acquisition method is not applicable to DC system. In view of this, the proposed usage of full-frequency electrical quantities is a new attempt to calculate DC line parameters and locate faults.

V. VALIDATION AND STUDY RESULTS

In the four MMC stations shown in Fig. 2, the converter station 3 uses constant DC voltage control and constant reactive power control, and the remaining converter stations adopt constant real power control and constant reactive power control. Note that, in order to limit the fault current and improve the fault ride-through capability of the DC grid, the smoothing reactors are installed at both ends of the DC lines. More detailed system parameters are given in Table I.

TABLE I
PARAMETERS OF THE VALIDATION SYSTEM AND MODEL

System parameters	Value
Line length (km)	Line 1: 227
	Line 2: 126
	Line 3: 219
	Line 4: 66
DC voltage (kV)	±500
Capacitance of SM (μF)	15000
Number of submodules	233
Smoothing reactor (mH)	150
Rated power of S_1 and S_2 (MW)	1500
Rated power of S_3 and S_4 (MW)	3000
r_0 (Ω/m)	3.3597×10^{-5}
l_0 (H/m)	1.2751×10^{-6}

The required settings include, fault occurs at 1.0s, the data sampling frequency is 50kHz synchronized at both ends, and the fault locations are from f_1 to f_{11} as marked in Fig. 2. The f_1-f_4 are internal fault points which locate at 20%, 40%, 60%, 80% of Line 1, f_6-f_{10} are also internal fault points which locate at 10%, 30%, 50%, 70% and 90% of Line 4, f_5 and f_{11} are respectively external faults of Line 1 and Line 4. The total data

window needed in this paper is 5ms.

The use of the first-order lag (low-pass filter) is to obtain a simplified and mathematical model of transmission lines (as shown in Fig. 4), which facilitates the derivation and analysis of the subsequent location algorithm. In the subsequent verification of the model accuracy and location algorithm, simulation studies (as shown Figs. 5-16) were carried out using the detailed model of the overhead lines representing the effects of frequency-varying characteristics and distributed capacitance, which was not simplified.

A. Validation of the Voltage Gradient Algorithm

When the MMC-MTDC system is running, the voltage data of two DC poles at the MMC bus bars are continuously detected, calculated and compared with the threshold value. Fig. 9 shows the values of the voltage gradient corresponding to pole-to-pole faults occurring at different locations of Line 4 and a negative-pole-to-ground (N-G) fault occurring at the midpoint of Line 4. Considering that after the pole-to-pole fault, the positive and negative voltages change in a consistent trend, hence Fig. 9 only shows the voltage gradient value of the positive pole, which is also the non-faulty pole when occurring N-G faults.
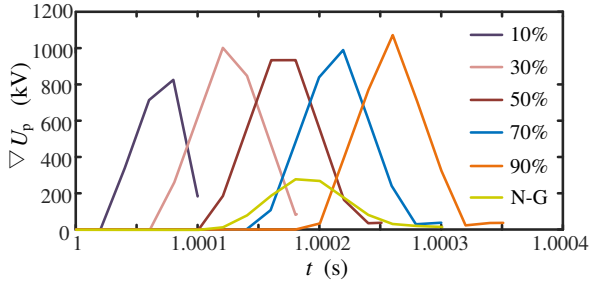

Fig. 9 The voltage gradient of positive pole corresponding to different faults.

It can be seen that the voltage gradient value of the faulted pole will reach a large value after fault occurrence compared to the healthy pole. The peak time varies slightly depending on the locations of the fault. Without loss of generality, the midpoint of the line is selected to test pole-to-pole faults under different operating conditions, aiming to find the proper threshold of the improved method. Fig. 10 shows the changing trend of the maximum value of the voltage gradient of positive pole with the changing of fault resistance, smoothing reactor size and transmitted real power of MMC.
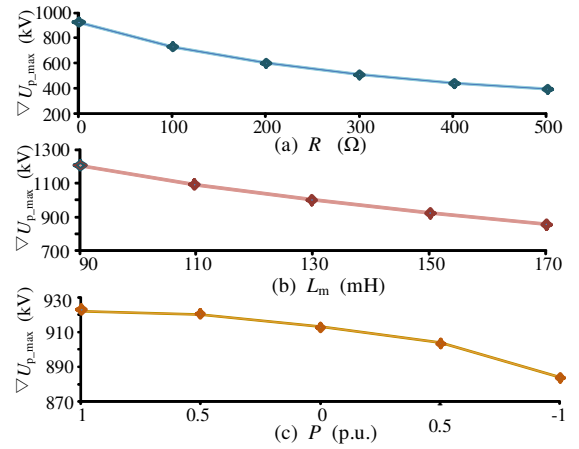

Fig. 10 The maximum value of the voltage gradient of positive pole: (a) fault resistance, (b) the smoothing reactors, (c) real power.

From Fig. 10, it is observed that the change of each parameter will change the maximum value of the voltage gradient, and among which the fault resistance having the greatest impact. For Line 4, the threshold of the voltage gradient method is chosen to be 400 kV, which can be applied to equation (1) to initiate the fault location algorithm when a pole-to-pole fault occurs. Different lines should be configured with specific thresholds due to different line lengths and transmitted power. The confirmation method of these threshold values is similar to Line 4.

B. Validation of the Proposed Included Angle Cosine

Section IV proposed the concept of included angle cosine, which uses current data from both ends to identify internal and external faults. Assuming pole-to-pole fault respectively occurs at internal fault points of Line 4 (f_6- f_{10}) and external fault point (f_{11}), the calculated results of the included angle cosine corresponding to different operating conditions are given in Table II.

TABLE II (A)
CALCULATED INCLUDED ANGLE COSINE

Fault location	Fault resistance (Ω)		
	0	300	500
f_6	-1	-0.97	-0.99
f_7	-1	-0.98	-0.99
f_8	-1	-0.99	-0.99
f_9	-1	-0.99	-0.98
f_{10}	-1	-0.97	-0.99
f_{11}	1	0.95	0.91

TABLE II(B)
CALCULATED INCLUDED ANGLE COSINE

	Smoothing reactor (mH)			Transmitted power (p.u.)		
	90	130	170	1.0	0	-1.0
f_6	-0.99	-1	-0.99	-1	-1	-1
f_7	-0.98	-0.98	-0.98	-1	-0.99	-1
f_8	-1	-1	-1	-1	-1	-1
f_9	-1	-1	-0.98	-1	-0.99	-1

| f_{10} | -1 | -0.99 | -1 | -1 | -0.98 | -1 |
| f_{11} | 0.98 | 0.96 | 0.99 | 1 | 0.99 | 0.98 |

It can be found that the values correspond to internal faults are close to '-1' while the values correspond to external faults are close to '1'. Therefore, by calculating the included angle cosine of current-deviations, it is possible to accurately identify the internal and external faults in the DC system.

Once the fault is determined to be an internal pole-to-pole type, the fault location coefficient algorithm proposed in this paper will be started. The voltage and current data will pass through a first-order lag represented as $\frac{G}{1+ST}$ (G = 1 and T = 0.002s).

C. The Validation of Pole-to-ground Short-circuit Fault Location Coefficient at Different Fault Points

The proposed fault location procedure also applies to P-G faults. The equivalent network after P-G fault is shown in Fig. 11.
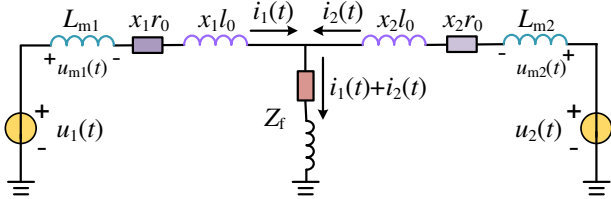

Fig.11 Model used for pole-to-ground fault location

The location coefficient η under P-G fault can be derived from the derivation of P-P fault, which is

$$\lambda(k) = \frac{L\left[r_0 i_2(k) + l_0 \frac{u_{m2}(k)}{L_{m2}}\right]}{L\left[r_0 i_1(k) + l_0 \frac{u_{m1}(k)}{L_{m1}} + r_0 i_2(k) + l_0 \frac{u_{m2}(k)}{L_{m2}}\right]}$$
$$+ \frac{u_1(k) - u_2(k) - u_{m1}(k) + u_{m2}(k)}{L\left[r_0 i_1(k) + l_0 \frac{u_{m1}(k)}{L_{m1}} + r_0 i_2(k) + l_0 \frac{u_{m2}(k)}{L_{m2}}\right]} \quad (16)$$

$$\min \sum_{k=1}^{n}\left[\lambda(k) - \eta\right]^2 \quad (17)$$

Using equations (16) and (17) and the calculated parameters r_0 and l_0, the fault location coefficient can be obtained, and location error is calculated by:

$$Error = \left|\eta - \frac{x_1}{L}\right| \times 100\% \quad (18)$$

Setting positive P-G faults at different locations of Line 1, the location results are shown in Table III.

TABLE III
P-G FAULT LOCATION RESULTS

Fault location	20%	40%	60%	80%
Location error(%)	1.1	0.5	0.3	0.7

P-G and P-P faults have similar fault equivalent networks, the same derivation process and approximate location expression. The test results show that the proposed location algo-

rithm has good applicability to P-G faults. Due to space limitations, this paper mainly proposes formula derivation and simulation verification for pole-to-pole faults.

D. The Validation of Pole-to-pole Short-circuit Fault Location Coefficient at Different Fault Points

Fig. 12 shows the corresponding results. The abscissa represents the actual fault locations, specifically the ratio of the distance between the fault point and one terminal of the line over the total line length. It includes nine internal fault points of two DC lines, which are f_1- f_4 and f_6- f_{10} respectively set within Line 1 and Line 4. The ordinate indicates the location error.
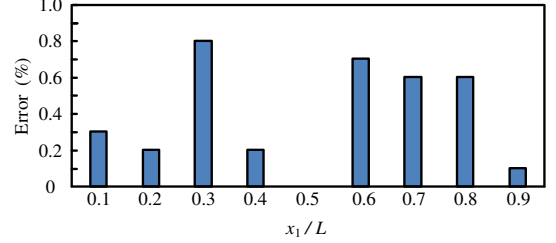

Fig. 12 Location errors of different short-circuit fault points.

It is seen that the location errors are smaller than 0.8%, which means location coefficients can accurately represent the actual fault location. Therefore, the location algorithm is sufficiently accurate, and not affected by the fault locations and the length of the DC lines.

E. Validation of the Location Accuracy under Various System Aspects

As indicated before, the fault resistance, smoothing reactor size and the transmitted real power have influences on the measured voltage and current data from both terminals of the DC lines. Therefore, it is necessary to check the impact of these aspects on the location accuracy. In this scenario, DC Lines 1 and 4 are used for the validations.
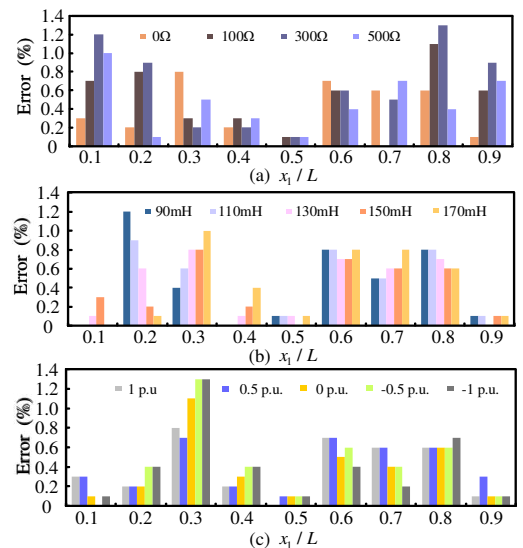

Fig. 13 Fault location error of different short-circuit fault points: (a) fault resistance, (b) smoothing reactors, (c) transmitted power.

Fig. 13(a) shows the location coefficient of nine

pole-to-pole short-circuit faults in Line 1 and Line 4 under different fault resistance and the effect of smoothing reactors is shown in Fig. 13(b). The results in Fig. 13(c) are obtained by changing the transmitted real power of the MMC station S1.

When these parameters change, the location errors do not change much and keep in a relatively small range. As indicated in the theoretical analysis, the use of two-terminal voltage and current data can eliminate the effects of fault resistance. Applying the measured voltage values from positive and negative poles, measured current values from the DC lines and the voltage drops across the smoothing reactors, the impact from the smoothing reactors and transmitted power can be minimized.

F. Validation of the Location Accuracy under Various System Aspects

Table IV and V show the location errors of faults at Line 1 and Line 4 respectively when the four-terminal system is under normal, n-1 and n-2 modes.

TABLE IV
EFFECTS OF VARIOUS OUTAGE MODES ON LOCATION ERRORS OF LINE 1

		Fault location			
	Location error (%)	20%	40%	60%	80%
Disconnected line	non	0.2	0.2	0.7	0.6
	Line 2	0.6	0.4	0.2	0.3
	Line 3	0.1	0.2	0.2	0.5
	Line 4	0.1	0.2	0.1	0.1
	Line 2, Line 3	0.5	0.7	0.8	0.5
	Line 2, Line 4	1.0	0.9	0.7	0.8
	Line 3, Line 4	0.3	0.5	0.2	0.3

TABLE V
EFFECTS OF VARIOUS OUTAGE MODES ON LOCATION ERRORS OF LINE 4

		Fault location				
	Location error (%)	10%	30%	50%	70%	90%
Disconnected line	non	0.3	0.8	0	0.6	0.1
	Line 1	0.3	0.7	0	0.4	0.3
	Line 2	0.5	0.8	0.1	0.5	0.8
	Line 3	1.2	1.9	0.1	0.6	0.8
	Line 1, Line 2	1.0	0.7	0	0.2	0.4
	Line 1, Line 3	0.7	1.2	0.1	0.9	0.7
	Line 2, Line 3	0.5	1.1	0	0.5	0.9

It can be found that under different outage modes, the algorithm can accurately locate faults at different locations of different lines, with the location error less than 1% in general. Therefore, the fault location algorithm is not affected by states of other lines. As this is an offline algorithm, all the status of system circuits, including breakers, have already been known by the control center and the algorithm has the function of fault detection, it is not necessary to communicate status of breakers to each controller.

G. The Effects of Synchronization Error and Sampling Frequency

The algorithm proposed in this paper needs to use the double-ended synchronous voltage and current data after sampling, so it is necessary to study the effects of synchronization error and sampling frequency on location accuracy. Taking faults of Line 1 as an example, Fig. 14 and Fig. 15 show the results.
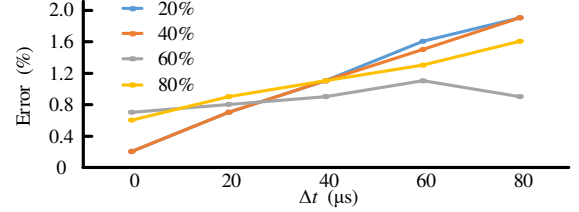

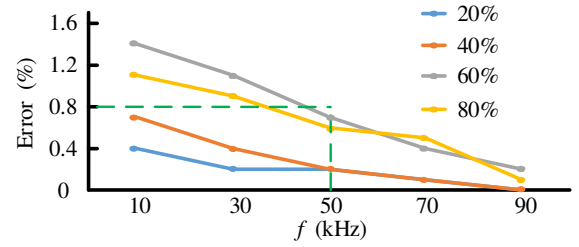Fig. 14 Effects of synchronization error

Fig. 15 Effects of sampling frequency

The location error increases as synchronization error increases, which exceeds 1% when the time difference of the double-ended signal is greater than 20μs. However, since the current GPS system can provide a common clock signal with a time synchronization accuracy of less than 0.1μs [7], the synchronization error is acceptable for the proposed method.

It can be seen from Fig. 15, the location error decreases as the sampling frequency increases, and has dropped below 1% at 50 kHz. Continue to increase the sampling frequency has a limited effect on improving location accuracy. Therefore, the sampling frequency in this paper is set to 50 kHz.

H. Noise Influence on Location Accuracy

Noise can cause fluctuations and randomness in the measured electrical quantity, taking the actual measurement of bipolar DC voltages (u_1) as an example to show the effect of 30dB noise, as shown in Fig.16.
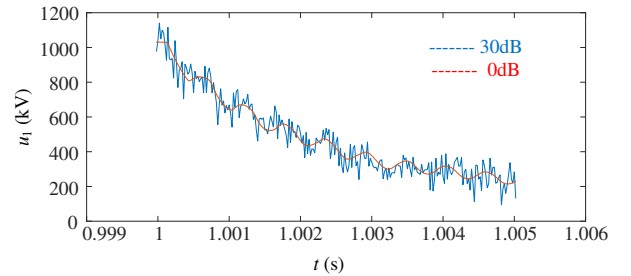

Fig.16 Measured DC voltage at the DC bus bars with noise

To investigate the influence of noise on location accuracy, the measured voltage and current data are contaminated with different levels of white Gaussian noise. In the test, the

intensity of the white Gaussian noise applied to voltage is six times the amount of current. Table VI gives the test results.

TABLE VI
EFFECTS OF NOISE ON LOCATION ACCURACY

		White Gaussian Noise (dB)						
Location error(%)		0	5	10	15	20	25	30
Fault location	20%	0.2	0.3	0.3	0.5	0.4	0.7	0.8
	40%	0.2	0.4	0.5	0.2	0	0.4	0.9
	60%	0.7	0.8	0.7	0.6	0.2	0.6	0.3
	80%	0.6	0.5	0.4	0.7	0.7	0.6	0.4

The increase in the intensity of white Gaussian noise does not necessarily cause an increase in the location error. This is because the white Gaussian noise itself has a certain randomness. In general, the presence of white Gaussian noise does not significantly affect the accuracy of the location algorithm. It can be seen that the location algorithm proposed in this paper has strong anti-noise ability.

The proposed method has the following advantages: it has strong tolerance to fault resistance and is almost unaffected by line boundary components, which are the drawbacks of travelling wave method. The limitations are as follows: precision of the proposed location method is not much higher than the travelling wave method and relatively lower sampling frequency seems not to significantly reduce the cost. The location algorithm of cable lines or transmission-cable hybrid lines has not been included yet and needs further study. Also, the proposed method and the traveling wave method require a comprehensive and in-depth comparison in terms of comprehensive technical and economic aspects.

VI. CONCLUSIONS

This paper proposes a location scheme with reduced computation to accurately identify fault type and location in a DC grid. Also, a simplified R-L representation is proposed to model a detailed frequency dependent transmission line by calculating the RL parameters for fault location. In this paper, the location algorithm of cable lines or transmission-cable hybrid lines has not been concluded, which needs further study.

The simplified representation does not need complicated algorithms to extract specific frequency components. And the sampling frequency is much lower than the traveling wave method and does not need to capture the travelling wave head.

The proposed algorithms are proven to be robust under various fault locations and are almost not affected by fault resistance, smoothing reactors, and the transmitted power.

ACKNOWLEDGMENT

REFERENCES

[1] T. An et al., "A DC grid benchmark model for studies of interconnection of power systems," *CSEE Journal of Power and Energy Systems*, vol. 1, no. 4, pp. 101-109, Dec. 2015.

[2] J. Liu, N. L. Tai and C. J. Fan, "Transient-Voltage-Based Protection Scheme for DC Line Faults in the Multi-terminal VSC-HVDC System," *IEEE Trans. Power Del.*, vol. 32, no. 3, pp. 1483-1494, Jun. 2017.

[3] T. An, G. Tang, and W. Wang, "Research and application on multi-terminal and DC grids based on VSC-HVDC technology in China," *IET High Voltage*, vol. 2, no. 1, pp. 1-10, 2017.

[4] L. Z. Yao, J. Wu, L. Xu and M. H. Rahman, "Studies of coordinated zone protection strategy for DC grid," in *Power Electronics & Motion Control Conference*, pp. 713-718, 2016.

[5] W. Su, Y. F. Gong and Y. Li, "Traveling-Wave-Based Line Fault Location in Star-Connected Multi-terminal HVDC Systems," *IEEE Trans. Power Del.*, vol. 27, no. 4, pp. 2286-2294, Jan. 2018.

[6] Q. Z. Lin, G. M. Luo, J. H. He, "Travelling-wave-based method for fault location in multi-terminal DC networks," *The Journal of Engineering*, vol. 2017, no. 13, 2017.

[7] OMKK Nanayakkara, AD Rajapaks and R Wachal, "Location of dc line faults in conventional HVDC systems with segments of cables and overhead lines using terminal measurements," *IEEE Trans. Power Del.*, vol. 27, no. 1, pp. 279-288, Nov. 2012.

[8] M Kong, X Pei, H Pang, J Yang, X Dong et al., "A lifting wavelet-based protection strategy against DC line faults for Zhangbei HVDC Grid in China," in *European Conference on Power Electronics and Applications*, pp. 1-11, 2017.

[9] D Yu, Y Li, Y Ding and X Zhang, "Fault Detection and Location for MTDC Combining Wavelet Analysis and Travelling Wave," in *Power Engineering & Automation Conference*, Sept. 2012.

[10] FV Lopes, "Settings-free traveling-wave-based earth fault location using unsynchronized two-terminal data," *IEEE Trans. Power Del.*, vol. 31, no. 5, pp. 2296-2298, Apr. 2016.

[11] J. Suonan, G. Song, and Q. Xu, "Time-domain fault location for parallel transmission lines using unsynchronized currents," *Elect. Power Energy Syst.*, vol. 28, no. 4, pp. 253–260, 2006.

[12] J Suonan, S Gao, G Song, Z Jiao and X Kang, "A Novel Fault-Location Method for HVDC Transmission," *IEEE Trans. Power Del.*, vol. 25, no. 2, pp. 1203-1209, Apr. 2010.

[13] BJ Rui, VA Lacerda, RM Monaro et al., "Selective non-unit Protection Technique for Multi terminal VSC-HVDC Grids," *IEEE Trans. Power Del.*, pp. 1-1, Sept. 2017.

[14] M Farshad, J Sadeh. "A novel fault-location method for HVDC transmission lines based on similarity measure of voltage signals," *IEEE Trans. Power Del.*, vol. 28, no. 4, pp. 2483-2490, Jul. 2013.

[15] ZY He, K Liao, XP Li et al., "Natural Frequency-Based Line Fault Location in HVDC Lines," *IEEE Trans. Power Del.*, vol. 29, no. 2, pp. 851-859, Apr. 2014.

[16] G. Song, J. Suonan, and Q. Xu, "Parallel transmission lines fault location algorithm based on differential component net," *IEEE Trans. Power Del.*, vol. 20, no. 4, pp. 2396–2406, Oct. 2005.

[17] S Azizi, M Sanaye-Pasand, M Abedini and A Hasani, "A Traveling-Wave-Based Methodology for Wide-Area Fault Location in Multi-terminal DC Systems," *IEEE Trans. Power Del.*, vol. 29, no. 6, pp. 2552-2560, Dec. 2014.

[18] R. D. Shultz and R. F. Gonzales, "Operating characteristics of an HVDC multi-terminal transmission line under single-pole faulted conditions and high resistance earth return," *Elect. Power Syst. Res.*, vol. 10, no. 2, pp. 103–111, 1986.

[19] J. Xu, C. Zhao, Y. Xiong, C. Li, Y. Ji and T. An, "Optimal Design of MMC Levels for Electromagnetic Transient Studies of MMC-HVDC," *IEEE Trans. Power Del*, vol. 31, no. 4, pp. 1663-1672, Aug. 2016.

[20] L. Tang and B.-T. Ooi, "Locating and isolating DC faults in multi-terminal DC system," *IEEE Trans. Power Del.*, 2007, vol.22, no. 3, pp.1877-1884.

[21] F Kong, Z Hao, S Zhang and B Zhang, "Development of a novel protection device for bipolar HVDC transmission lines," *IEEE Trans. Power Del.*, vol. 29, no. 5, pp. 2270-2278, Oct. 2014.

[22] J. P. Zhou, C. Y. Zhao et al, "Pilot Protection Method for DC Lines Based on Included Angle Cosine of Fault Current Component," *Automation of Electric Power Systems*, vol 42, no 14, pp 165-171, Jul. 25, 2018.

[23] J Yang, JE Fletcher and J O'Reilly. "Short-Circuit and Ground Fault Analyses and Location in VSC-Based DC Network Cables," *IEEE Trans. Ind. Elec.*, vol. 59, no. 10, pp. 3827-3837, Oct.2012.

[24] C Li, C Zhao, J Xu et al., "A Pole-to-Pole Short-Circuit Fault Current Calculation Method for DC Grids," *IEEE Trans. Power Sys.*, vol. 32, no. 6, pp. 4943 - 4953, Nov. 2017.

[25] K. Jia, M. Li, T. Bi et al., "Modified R-L model-based protection for VSC-DC distribution lines," *The Journal of Engineering*, vol. 13, no. 2017, pp. 1843 - 1846, 2017.

[26] D Yildiz, S Karagol and O Ozgonenel. "Estimation of Online Transmission Line Parameters and Fault Location by Using Different Differential Equation Algorithms," *Conference on Electrical and Electronics Engineering*, vol. 542, no. 3, pp. 1034-1038, Nov. 2015.

[27] J. Xu, S. Zhu, C. Li and C. Zhao, "The Enhanced DC Fault Current Calculation Method of MMC-HVDC Grid with Fault Current Limiters," *IEEE Journal of Emerging and Selected Topics in Power Electronics*, doi: 10.1109/JESTPE.2018.2888931, early access.

[28] J. Guo, G. Wang, Y. Liang and D. Zeng, "Global-Sensitivity-Based Theoretical Anal-ysis and Fast Prediction of Traveling Waves With Respect to Fault Resistance on HVDC Transmission Lines," in IEEE Transactions on Power Delivery, vol. 30, no. 4, pp. 2007-2016, Aug. 2015.

[29] X. Lin, F. Zhao, G. Wu, Z. Li and H. Weng, "Universal Wave front Positioning Correction Method on Traveling-Wave-Based Fault-Location Algorithms," in IEEE Transactions on Power Delivery, vol. 27, no. 3, pp. 1601-1610, Jul. 2012.

[30] S. Azizi, M. Sanaye-Pasand, M. Abedini and A. Hasani, "A Traveling-Wave-Based Methodology for Wide-Area Fault Location in Multiterminal DC Systems," in IEEE Transactions on Power Delivery, vol. 29, no. 6, pp. 2552-2560, Dec. 2014.

Jianzhong Xu (M'14-SM'19) was born in Shanxi, China. He received the B.S. and Ph.D. degrees from North China Electric Power University (NCEPU) in 2009 and 2014 respectively. Currently, he is an associate professor of the State Key Laboratory of Alternate Electrical Power System with Renewable Energy Sources, NCEPU. From 2012 to 2013, and 2016 to 2017, he was respectively a joint Ph.D. student and Post-Doctoral Fellow (PDF) at the University of Manitoba, under supervision of Prof. Ani Gole (IEEE Fellow). He is now working on the high-speed equivalent modeling, transient analysis of MMC-HVDC grid.

Yu Lü was born in Zhejiang, China. She received the B.S. degree from North China Electric Power University in 2018, where she is currently working toward her master degree. Her research interests include HVdc grid operation and protection.

Chengyong Zhao (M'05-SM'15) was born in Zhejiang, China. He received the B.S., M.S. and Ph.D. degrees in power system and its automation from NCEPU in 1988, 1993 and 2001, respectively. He was a visiting professor at the University of Manitoba from Jan. 2013 to Apr. 2013 and Sep. 2016 to Oct. 2016. Currently, he is a professor at the School of Electrical and Electronic Engineering, NCEPU. His research interests include HVDC system and DC grid.

Jun Liang (M'02-SM'12) received the B.Sc. degree from Huazhong University of Science and Technology, Wuhan, China, in 1992 and the M.Sc. and Ph.D. degrees from China Electric Power Research Institute, Beijing, China, in 1995 and 1998, respectively. From 1998 to 2001, he was a Senior Engineer with China Electric Power Research Institute. From 2001 to 2005, he was a Research Associate at Imperial College, London, U.K. From 2005 to 2007, he was a Senior Lecturer at the University of Glamorgan, Wales, U.K.. Currently, he is a Professor at the School of Engineering, Cardiff University, Wales, U.K. His research interests include FACTS devices/HVDC, power system stability and control, power electronics, and renewable power generation.